Appendix B

STATISTICAL ANALYSIS OF SQUEEZING

Here I describe the analytical methods we used to estimate the amount of squeezing measured with the on-chip balanced homodyne detectors in Chapters 2 and 6. First, I summarize common techniques for the measurement and analysis of squeezed light. I then motivate a statistical approach to the analysis of squeezed light. I introduce a statistical estimator for squeezing and antisqueezing levels that is robust to noise. I validate this estimator by developing a theoretical model, conducting experimental tests with a fiber-optic setup, and performing numerical simulations over the range of efficiency and squeezing parameters used in the on-chip squeezing experiments.

B.1 Background

Balanced homodyne detection is a standard measurement technique for the characterization of squeezed light [1]. A typical setup for the measurement of squeezed light is shown in Fig. B.1, where the signal at the output of balanced homodyne detector is proportional to the quadrature of the input optical field. There are two common approaches to the analysis of squeezing with balanced homodyne detection [1]. In the time-domain approach, output current or voltage statistics are accumulated over time with a time-resolving device, such as an oscilloscope, and quadrature statistics of the optical field are calculated in post-processing. In the frequency-domain approach, the output noise power spectrum is measured with an electronic spectrum analyzer, providing a direct measurement of a signal proportional to the quadrature variance of the optical field.

Squeezing can be characterized in the time-domain approach by acquiring quadrature samples for known phases over many rotations and performing quantum state tomography [2]. With optical homodyne tomography [3], the Wigner function of the squeezed state can be estimated by applying a reconstruction algorithm such as an inverse Radon transformation, maximum-entropy reconstruction, or maximum-likelihood estimation to time-domain data [4]. The squeezing and antisqueezing levels can be estimated by comparing the reconstructed Wigner function of the squeezed state to that of the vacuum state. In particular, the squeezing parameter and efficiency can be found from a fit to the Wigner function of the squeezed state [5]. However, these approaches are computationally intensive and depend on assump-

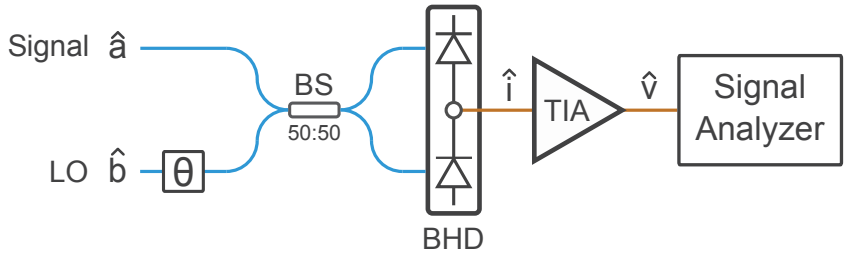

Figure B.1: Measurement of squeezed light with balanced homodyne detection. Squeezed light (signal) is interfered with strong local oscillator (LO) in a coherent state by a 50:50 beamsplitter (BS). A phase shifter on the LO controls the relative phase (θ) of the signal and LO. The mixed fields are detected with a balanced homodyne detector (BHD). The output current is amplified by a transimpedance amplifier (TIA), and the output voltage is sent to a signal analyzer, such as an oscilloscope or electronic spectrum analyzer.

tions in the reconstruction algorithm. While detection efficiency can be corrected for by means of an inverse Bernoulli transform [6], performance of such algorithms suffer for high detection loss. Moreover, numerical artifacts such as ripples in the reconstructed Wigner functions can obscure the squeezing level estimation [7].

With data measured in the time or spectral domain, squeezing and antisqueezing levels can be estimated from the minima and maxima of the normalized quadrature variances relative to the shot noise level. By fixing the relative phase between the LO and signal, sample quadrature variances in the time-domain approach or noise powers in the frequency-domain approach can be averaged over time to obtain squeezing or antisqueezing level estimates [1, 8]. Phase noise from stochastic phase fluctuations introduced in the measurement setup or imperfect phase-locking can result in averaging over various quadrature phases over the measurement time, which degrades the accuracy of squeezing estimation [9]. Alternatively, by modulating the phase of the LO, peak search methods may be applied to extract the squeezing levels [10, 5]. However, peak-searching methods are known to introduce statistical bias in the presence of noise, which can can skew the estimation of squeezing and antisqueezing levels in the presence of experimental noise sources [11, 12].

Here I introduce a method for the estimation of squeezing based on the probability density function of the quadrature sample variances. In Section B.2, I review balanced homodyne detection of squeezed light. I illustrate the observation of squeezing in both approaches by performing numerical simulations of squeezing in

the time-domain approach and experimental detection of squeezing in the frequency domain approach. In Section B.3, I develop a theoretical model for the probability density function of squeezed quadrature variances over a uniform phase distribution that accounts for sampling noise. In Section B.4, I demonstrate how the inflection points of the probability distribution of quadrature sample variances can be used as estimators of squeezing and antisqueezing. This approach allows for the estimation of squeezing without phase locking, in the presence of experimental noise sources such as phase and sampling noise. I then illustrate this method with numerical simulations and experimental measurements of squeezed light. This method is suitable for estimating squeezing levels comparable to the distribution of shot noise powers, relevant in the limit of low squeezing strength and high measurement loss.

B.2 Measurement of squeezing

Balanced homodyne detection

In balanced homodyne detection, squeezed light is mixed with a strong local oscillator and sent to a balanced homodyne detector (BHD). The output signal is a current or voltage proportional to the phase-dependent quadrature, $\hat{Q}_\theta$, of the signal field,

$$\hat{v}(\theta) \propto \beta \hat{Q}_\theta, \tag{B.1}$$

where the quadrature angle, θ, is the relative phase of the LO and the signal, β is the LO amplitude, and

$$\hat{Q}_\theta = \frac{1}{\sqrt{2}}(\hat{a}e^{-i\theta} + \hat{a}^\dagger e^{i\theta}) = \hat{Q}\cos\theta + \hat{P}\sin\theta, \tag{B.2}$$

where $\hat{a}$ is the signal field and $\hat{Q}$ and $\hat{P}$ are the canonical quadrature observables satisfying $[\hat{Q}, \hat{P}] = i$ [1, 13].

The output signal is sent to a signal analyzer that measures the time or frequency response of the voltages. Each voltage corresponds to a quadrature observable Q_θ, the eigenvalue of $\hat{Q}_\theta$ with eigenstate $|Q_\theta\rangle$. For a signal field in a Gaussian state $|\psi\rangle$, such as a vacuum, thermal, or squeezed state [14, 13], the quadrature observables are normally distributed according to,

$$|\psi(Q_\theta)|^2 = \frac{1}{\sqrt{2\pi}\langle\Delta\hat{Q}_\theta^2\rangle} \exp\left(-\frac{\left(Q_\theta - \langle\hat{Q}_\theta\rangle\right)^2}{2\langle\Delta\hat{Q}_\theta^2\rangle}\right) \tag{B.3}$$

where $\psi(Q_\theta) = \langle Q_\theta|\psi\rangle$ is the wavefunction in the phase quadrature basis, $\langle\hat{Q}_\theta\rangle = \langle\psi|\hat{Q}_\theta|\psi\rangle$ is the quadrature mean and $\langle\Delta\hat{Q}_\theta^2\rangle = \langle\psi|\Delta\hat{Q}_\theta^2|\psi\rangle$ is the quadrature variance.

For a field in a vacuum state, $\langle \hat{Q}_\theta \rangle = 0$ and $\langle \Delta \hat{Q}_\theta^2 \rangle = 1/2$. For a field in a squeezed state, the quadrature variance is given by,

$$\langle \Delta \hat{Q}_\theta^2 \rangle_{\text{sq}} = \frac{1}{2}(e^{-2r} \cos^2 \theta + e^{2r} \sin^2 \theta), \tag{B.4}$$

where r is the squeezing parameter. Decoherence is modeled as a virtual beamsplitter transformation that mixes the signal field with a vacuum mode,

$$\hat{a} \mapsto \sqrt{\eta}\hat{a} + \sqrt{1-\eta}\hat{a}_{\text{vac}}, \tag{B.5}$$

where η is the transmittance of the virtual beamsplitter. In the presence of decoherence, the quadrature variance of a squeezed vacuum state becomes,

$$\langle \Delta \hat{Q}_\theta^2 \rangle_{\text{sq}} = \frac{\eta}{2}(e^{-2r} \cos^2 \theta + e^{2r} \sin^2 \theta) + \frac{1-\eta}{2}, \tag{B.6}$$

where η represents the total measurement efficiency include effects of optical loss and electronic noise [15].

The amount of squeezing can be characterized experimentally by comparing the variance of the quadratures measured with a squeezed state input to that measured with a vacuum state input,

$$\frac{\langle \Delta \hat{Q}_\theta^2 \rangle_{\text{sq}}}{\langle \Delta \hat{Q}_\theta^2 \rangle_{\text{vac}}} = \eta(e^{-2r} \cos^2 \theta + e^{2r} \sin^2 \theta) + 1 - \eta, \tag{B.7}$$

where the squeezing and antisqueezing levels relative to the shot noise level, $\eta e^{\pm 2r} + 1 - \eta$, occur at $\theta = 0$ and $\theta = \pi/2$, respectively.

Time-domain approach

Using a time-domain analyzer in the setup in Fig. B.1, squeezing can be characterized by sweeping the LO phase and accumulating voltage statistics for various phases. A numerical simulation of quadrature samples accumulated over time for a linear phase ramp applied to the LO is shown in Fig. B.2. An array of 10^5 phases is generated from 0 to 4π. For each phase, a quadrature observable is sampled from a Gaussian distribution described by Eq. B.3 to obtain a total set of 10^5 quadrature samples. The samples for a vacuum state (orange) and a squeezed vacuum state (blue) with $r = 1$ and $\eta = 0.8$ are shown in Fig. B.2a. To obtain sample mean and variances, the total sample set is divided into subsets of 1000 samples, and the mean and variance is calculated for each subset. The sample mean and variance as function of time (phase) are shown in Fig. B.2b and c, respectively.

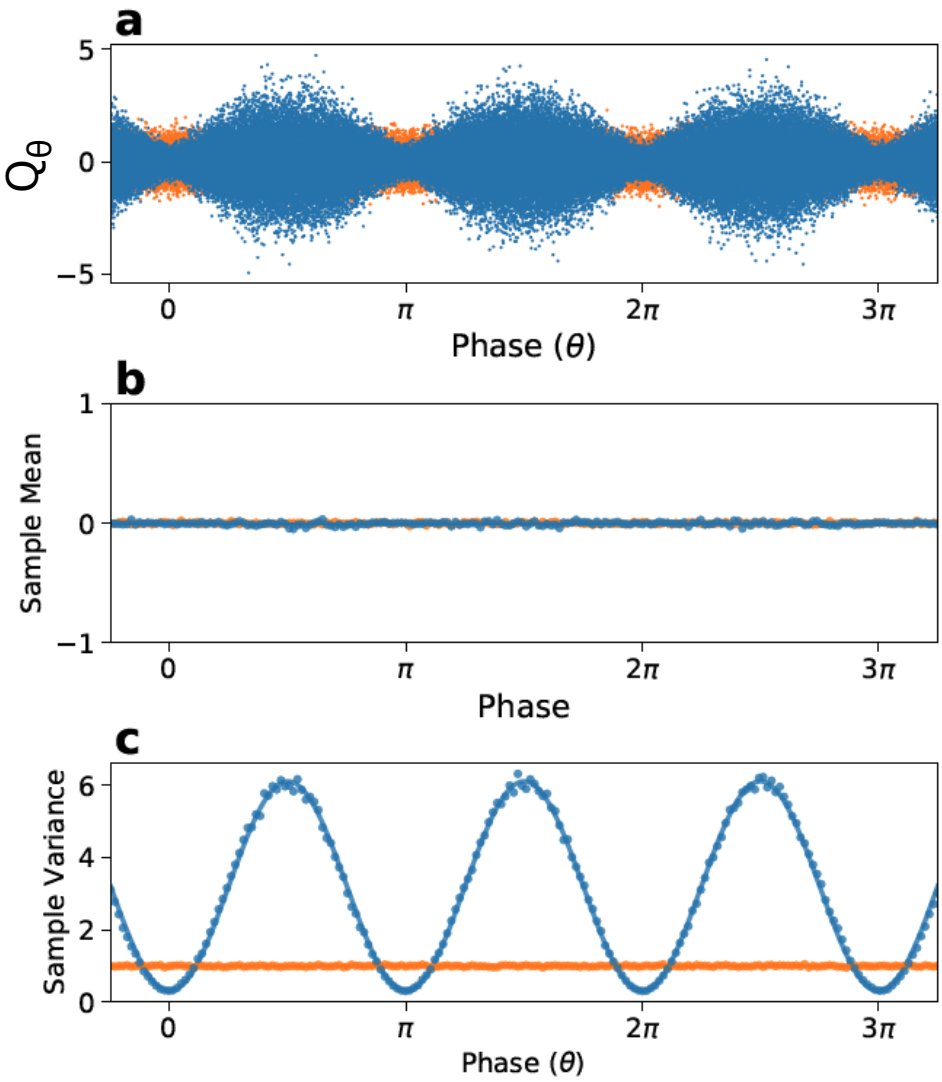

Figure B.2: Numerical simulation of quadrature statistics obtained from time-domain analyzer for a linear phase ramp applied to the LO. a) Quadrature samples as a function of time (phase) for a vacuum state (orange) and a squeezed vacuum state with $r = 1$ and $\eta = 0.8$ (blue). b) Sample means and c) normalized sample variances as a function of time. The sample variances are normalized to the mean of the vacuum sample variances. The solid lines in b) and c) are the corresponding analytic predictions for the quadrature means and variances.

Frequency domain approach

Alternatively, by using an electronic spectrum analyzer in the setup of Fig. B.1, noise power levels can be measured directly in real-time. Squeezed vacuum states of light are experimentally generated and the noise powers are measured over time using a fiber-coupled BHD. The experimental setup is shown in Fig. B.3a. Laser light at telecom wavelength of 1550 nm is split into signal path and local oscillator (LO) path. In the signal path, the light amplified by an erbium doped fiber amplifier (EDFA) and upconverted to 775 nm by second harmonic generation (SHG) by a periodically poled lithium niobate (PPLN) waveguide. The 775 nm light is used as a pump for spontaneous parametric down conversion (SPDC) by another PPLN waveguide to generate squeezed vacuum light. The pump power is controlled by tuning the gain of EDFA to vary the amount of squeezing. The squeezing parameter $r = \mu\sqrt{P}$ is related to the square root of the pump power (P) by the proportionality constant μ, which depends on the strength of the nonlinearity of the PPLN waveguide. A PPLN waveguide with $\mu = 0.038\ [\mathrm{mW}]^{-1/2}$ is used for SPDC. The squeezed light is sent through an isolator, which acts as a filter for residual 775 nm pump light and rejects backreflected light, followed by interference with the LO at a 50:50 beamsplitter for balanced homodyne detection. In the LO path, laser light is phase modulated by a lithium niobate electro-optic modulator to vary the relative phase between the signal and LO. The outputs of BS are sent to fiber-coupled balanced photodiodes, and the RF output of the BHD is sent to a RF spectrum analyzer.

Examples of noise power traces measured with the RF spectrum analyzer are shown in Fig. B.3 for various squeezing parameters and video bandwidths (VBWs). The blue traces correspond to squeezed vacuum states and the orange traces correspond to the vacuum state. Squeezed vacuum states are generated with squeezing parameters of $r = 0.35$ in Fig. B.3b,c and $r = 0.06$ in Fig. B.3d,e, corresponding to 3.04 dB and 0.52 dB generated squeezing, respectively, with a net measurement efficiency is $\eta = 0.326$. A $0-2\pi$ phase ramp at a 1 Hz modulation frequency is applied to the LO. The non-uniform phase fluctuations are due to thermal and mechanical drifts in the fiber optics, which introduce relative phase shifts between the LO and signal paths. A peak search algorithm is applied to extract minima and maxima in the squeezing data relative to the mean shot noise level. The squeezing and antisqueezing levels are obtained from the arithmetic mean of the minima and maxima, respectively (red dashed lines). The mean squeezing (antisqueezing) levels are b) -0.75 ± 0.02 (1.16 ± 0.01) dB, c) -0.78 ± 0.03 (1.20 ± 0.02) dB, d) -0.17 ± 0.01 (0.18 ± 0.01) dB, and e) -0.21 ± 0.01 (0.21 ± 0.01) dB relative to the mean shot noise level.

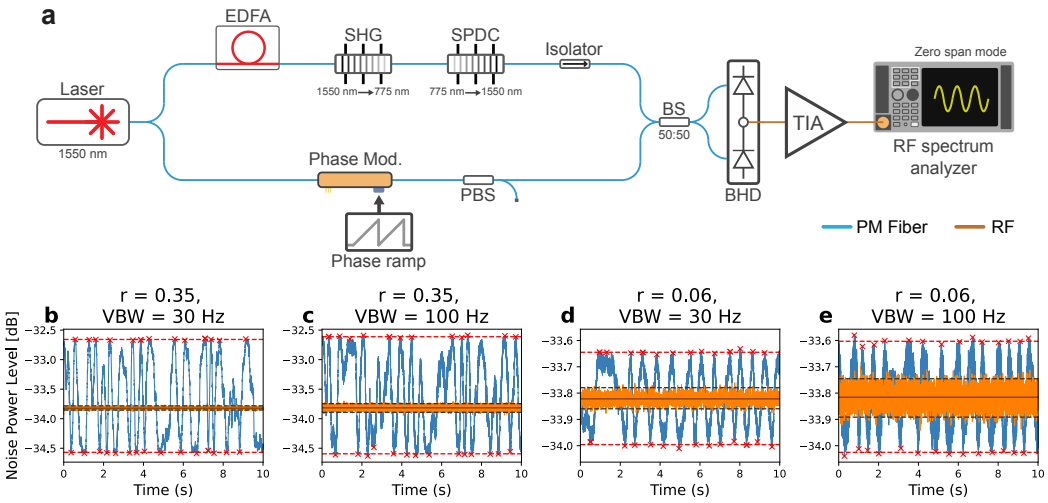

Figure B.3: Generation and measurement of squeezed light. a) Experimental setup. EDFA: erbium doped fiber amplifier, SHG: second harmonic generation, SPDC: spontaneous parametric downconversion, PBS: polarizing beamsplitter, BS: polarization maintaining beamsplitter, BHD: balanced homodyne detection, TIA: transimpedance amplifier. b-e) Experimental noise power traces of squeezed light measured with an RF spectrum analyzer. The traces are measured on zero span mode with a central frequency of 8 MHz, a resolution bandwidth (RBW) of 2 MHz, and sampling rate of 10 kHz over 10 seconds. The traces in b) and d) are measured with a video bandwidth (VBW) of 30 Hz and the traces in c) and e) are measured with a VBW of 100 Hz. The squeezing parameters are $r = 0.35$ for b) and c) and $r = 0.06$ for d) and e), with a net measurement efficiency of $\eta = 0.326$. Peaks in the squeezed light data extracted using a peak search algorithm are indicated with red markers, and the mean of the markers are indicated with dashed red lines. The same peak search algorithm is applied to the vacuum data, where the mean peak power levels are indicated by dashed black lines. The solid black lines are the mean power levels of the vacuum data.

The uncertainties on the squeezing and antisqueezing estimates are obtained from the standard deviation of minima and maxima, respectively. The same algorithm is applied to the vacuum data to obtain lower and upper bounds on the shot noise power distribution (black dashed lines). The peak search algorithm estimates upper and lower bounds of ±0.04 dB and ±0.07 dB for vacuum data taken with 30Hz and 100Hz VBW, respectively.

Shot noise power distribution

In the aforementioned methods, stable measurement of the vacuum state, that is, the shot noise level, is required for accurate estimation of squeezing. While the quadrature variance of the vacuum state is theoretically a constant (1/2), in practice, the measured variances are distributed as seen in Fig. B.3. The variance of the shot noise power distribution sets the limit on the minimum amount of squeezing that can be resolved. One possible cause for the distribution in the vacuum quadrature variances observed experimentally is optical gain instability, for example from imperfect cancellation of classical noise such as LO power fluctuations. This could be due to unbalanced detectors or imperfect LO and signal interference. Prominent in the low squeezing and high measurement loss regime, LO power fluctuations can cause significant variations in the shot noise level even for high squeezing and low measurement loss [16]. Such instabilities can be mitigated by optimizing the common mode rejection ratio (CMRR) [8], with up to 90 dB CMRR (Chapter 6) demonstrated by us in the literature.

Another cause for shot noise level uncertainty is sampling noise. Sampling noise bounds the width of the shot noise power distribution and sets the minimum amount of squeezing that can be resolved experimentally. For the time-domain approach, the quadrature sample sizes are determined by the sampling rate of the measurement. The sampling rate should be much higher than the LO phase modulations in order to obtain sufficiently high sample sizes for the calculation of the sample variances over multiple phases. In the frequency-domain approach, the sampling bandwidth is controlled with the amount of spectral and temporal filtering performed by the IF and video filters inside the spectrum analyzer [17]. Filtering can also be implemented in the time-domain approach with digital signal processing.

The effect of the shot noise power distribution on the estimation of squeezing levels is illustrated by the frequency-domain data in Fig. B.3. Since the measurements are performed with $\geq$ 30 dB CMRR, corresponding to shot noise power levels

with $\leq 0.1\%$ power fluctuations, optical gain instability is negligible relative to the sampling bandwidth. Peak searching can provide reasonable estimates for the squeezing and antisqueezing levels when the widths of the distributions are small relative to the squeezing and antisqueezing levels. However, for non-negligible widths, peak search methods overestimate the squeezing and antisqueezing levels. The overestimation in the squeezing and antisqueezing levels becomes clear for low squeezing parameters in Fig. B.3 d and e. The estimated squeezing levels depend on the width of the shot noise power distribution and are capped at the upper and lower bounds of the vacuum data, set by the sampling bandwidths.

B.3 Theoretical model

Sampling noise

To account for the effect of sampling uncertainty on the estimation of squeezing, I develop a theoretical model for the distribution of squeezed quadrature variance in the presence of sampling noise. Since the quadrature observables of Gaussian states are normally distributed, Cochran's theorem can be applied to find the probability density functions (PDFs) of the sample quadrature variance distributions for the vacuum state and squeezed state at a fixed phase. Following Cochran's theorem [18], the sample variance of n samples of a normal distribution with standard deviation σ is a random variable (S^2) that is chi-squared distributed,

$$S^2 \sim \Delta Q^2 \frac{\chi^2_{n-1}}{n-1}, \tag{B.8}$$

where χ^2_{n-1} is the chi-squared distribution with $n-1$ degrees of freedom. The sample variance distribution has mean Q^2 and approaches a normal distribution for large n.

In the frequency-domain approach, the noise powers are distributed as Eq. B.8, where the width of the distribution is set by sampling bandwidths, e.g. RBW and VBW. The powers acquired by spectrum analyzers are commonly reported in decibel (dB) scale. A statistical feature of this is that the distribution of noise powers in logarithmic scale converges faster to a normal distribution than in linear scale, and the width of the distribution is independent of the power level, see Fig. B.4e and f. This follows from Eq. B.8, as $\ln(\chi^2)$ converges to normality much faster than χ^2, and $\ln S^2 - \ln \sigma^2$ is independent of σ^2 [19].

In Fig. B.4a-d, I compare the PDFs obtained by from Eq. B.8 with a numerical simulation in the time-domain approach. With a sample size of $n = 100$, the

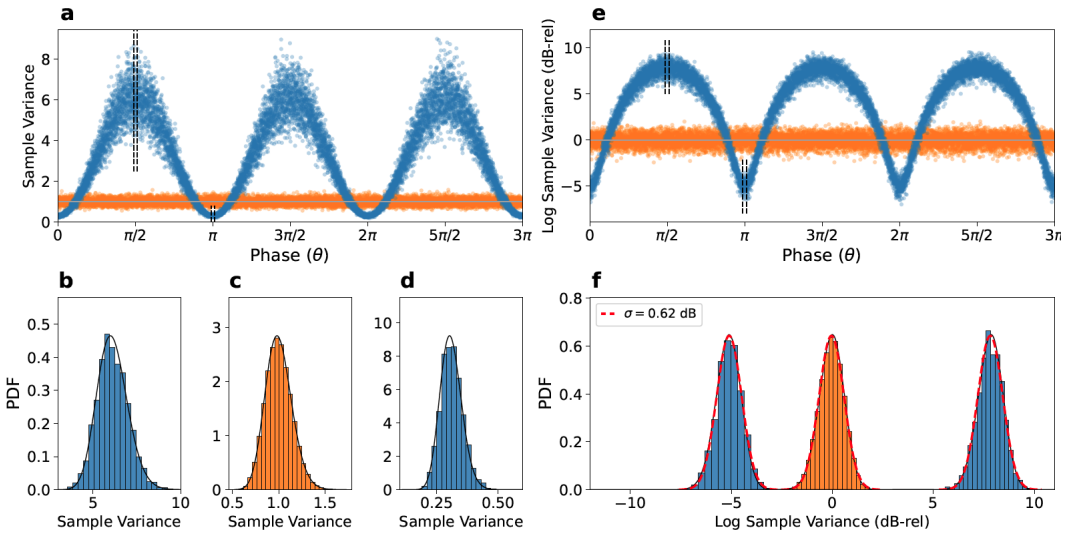

Figure B.4: Sample quadrature variance statistics in linear and logarithmic scales. a) Same simulation as in Fig. B.2 but with a $5e6$ quadrature samples of the vacuum state (orange) and squeezed vacuum state with $r = 1$ and $\eta = 0.8$ (blue) over a period. Sample variances are reported relative to the mean shot noise level. Sample variances are calculated over subsets of $n = 100$ samples. Histograms of the sample variances for b) the squeezed state at $\theta = \pi/2$, c) the vacuum state, and d) the squeezed state at $\theta = \pi$. The black lines are the corresponding theoretical predictions from obtained from Cochran's theorem in Eq. B.8. e) Simulation in a) plotted in logarithmic scale, relative to the mean shot noise level. f) Histograms of the log-scale sample variances for (left) the squeezed state at $\theta = \pi/2$, (middle) the vacuum state, and (right) the squeezed state at $\theta = \pi$. The histograms are fitted to Gaussian distributions, each with standard deviation $\sigma = 0.62$ dB. The log-scale histograms approach normality faster than the linear-scale histograms and have the same standard deviation for each phase, unlike in linear scale.

sample variances of the vacuum state are approximately normally distributed. For the squeezed state, the sample variances are approximately normally distributed for each phase, where the width scales with $Q^2 = \langle \hat{Q}_\theta^2 \rangle_{\text{sq}} / \langle \hat{Q}_\theta^2 \rangle_{\text{vac}}$.

Probability density function

Let $X \equiv S_\theta^2 / \langle \Delta \hat{Q}_\theta^2 \rangle_{\text{vac}}$ denote the quadrature sample variance, S_θ^2, normalized by the quadrature variance of the vacuum state, $\langle \Delta \hat{Q}_\theta^2 \rangle_{\text{vac}} = 1/4$. X is a random variable whose probability distribution (PDF), $f(X)$, is given by $f(X) = \delta(X - 1)$ for the

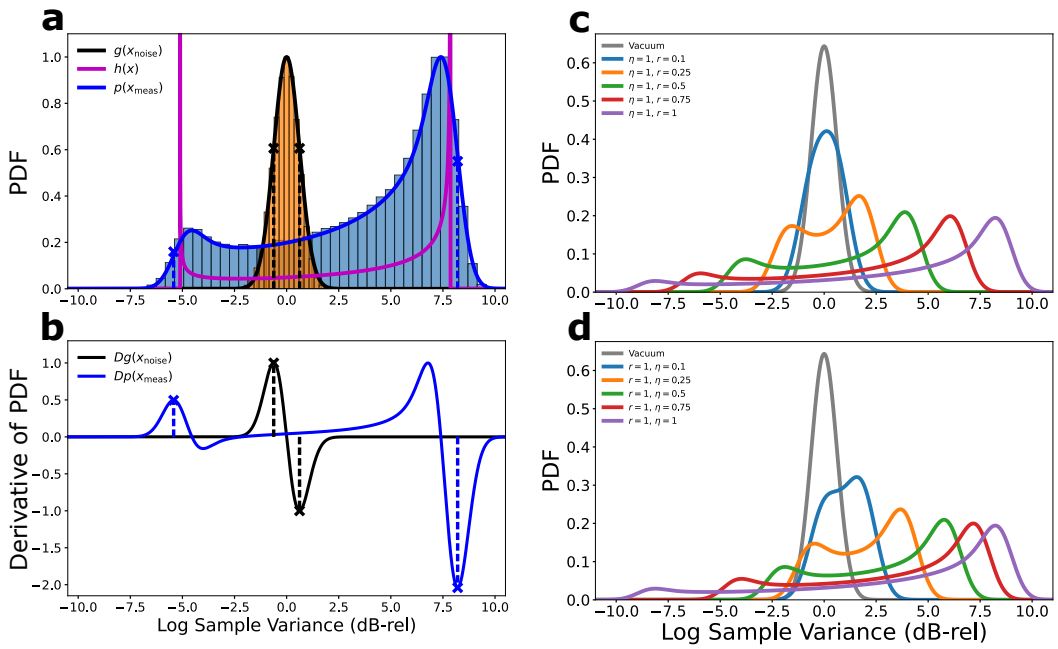

Figure B.5: Theoretical modeling for PDFs of logarithmic-scale quadrature variances sampled from a uniform phase distribution. a) PDF model for $r = 1$, $\eta = 0.8$, and a shot noise power distribution with a standard deviation of $\sigma = 0.62$ dB. The measured PDF, $p(x_{\text{meas}})$, is modeled as the convolution of the analytical squeezed vacuum PDF for uniform phase distribution, $h(x)$, with a Gaussian noise distribution, $g(x_{\text{noise}})$. The models for $g(x_{\text{noise}})$ and $p(x_{\text{meas}})$ are compared with histograms from a time-domain simulation of squeezed vacuum quadrature statistics for $r = 1$, $\eta = 0.8$, and $\sigma = 0.62$ dB. The inflection points of $g(x_{\text{noise}})$ and $p(x_{\text{meas}})$ are indicated with black and blue crosses, respectively. b) Derivatives of the PDFs for $g(x_{\text{noise}})$ and $p(x_{\text{meas}})$. The inflection points are identified from the left-most maximum and right-most minimum in the PDF derivatives, are indicated with black and blue crosses for $g(x_{\text{noise}})$ and $p(x_{\text{meas}})$, respectively. c) Measured squeezed vacuum PDF, $p(x_{\text{meas}})$, for various squeezing parameters, unit efficiency, and $\sigma = 0.62$ dB. d) Measured squeezed vacuum PDF, $p(x_{\text{meas}})$, for $r = 1$, various efficiencies, and $\sigma = 0.62$ dB.

vacuum state and

$$f(X) = \frac{1}{\pi\sqrt{(\eta \sinh 2r)^2 - (\eta \cosh 2r + 1 - \eta - X)^2}} \tag{B.9}$$

for the squeezed vacuum state. Eq. B.9 assumes that the quadratures are sampled over a uniform phase distribution.

To account for measurement noise, I model the measured quadrature sample variance as the random variable $x_{\text{meas}} = x + x_{\text{noise}}$, where $x \equiv 10\log_{10}(X)$ is the random variable for the quadrature sample variance in logarithmic scale, whose PDF is denoted by $h(x)$, and x_{noise} is the random variable that models the measurement noise, whose PDF is a Gaussian distribution with standard deviation σ,

$$g(x_{\text{noise}}) = \frac{1}{\sqrt{2\pi}\sigma} \exp\left(\frac{-x_{\text{noise}}^2}{2\sigma^2}\right). \tag{B.10}$$

Since x and x_{noise} are assumed to be mutually independent, the PDF of x_{meas}, $p(x_{\text{meas}})$, is the convolution of $h(x)$ and $g(x_{\text{noise}})$,

$$p(x_{\text{meas}}) = (h * g)(x_{\text{meas}}) = \int_{-\infty}^{\infty} h(x)g(x_{\text{meas}} - x)dx. \tag{B.11}$$

For the vacuum state, $h(x) = \delta(x)$. Therefore, the measured PDF of the vacuum state is $p(x_{\text{meas}}) = g(x_{\text{meas}})$, which corresponds to the shot noise power distribution. For the squeezed vacuum state, $h(x) = f(X(x))|X'(x)|$, where $f(X)$ is given by Eq. B.9 and $X(x) = 10^{x/10}$.

The convolved PDFs of the logarithmic sample variance for the vacuum state, $g(x_{\text{noise}})$, and squeezed vacuum state, $p(x_{\text{meas}})$, for $r = 1$ and $\eta = 0.8$ are shown in Fig. B.5a. The convolved PDFs are compared with the noiseless PDF, $h(x)$, for the squeezed vacuum state. In $h(x)$, the squeezing and antisqueezing levels are well-defined by the sharp edges of the distribution, due to the finite domain of Eq. B.9. The convolution of $h(x)$ with $g(x_{\text{noise}})$ smears out the PDF, causing the squeezing and antisqueezing levels to be poorly defined by the blurred edges. The convolved PDFs are plotted in Fig. B.5c for various squeezing parameters with unit efficiency and B.5d various efficiencies with squeezing parameter $r = 1$.

B.4 Estimation of squeezing

Estimation procedure

The left and right boundaries of the quadrature sample variance PDF are a natural choice of estimator for the squeezing and antisqueezing levels in the noiseless limit,

since the arcsine distribution of squeezed quadrature variances is sharply bounded (see Fig. B.5a). Here I use the inflection points of the quadrature sample variance PDF as estimators for the squeezing and antisqueezing levels in the presence of noise. These estimators provide a well-defined measure of the width of PDFs in the presence of unknown noise sources, motivated by the definition of the standard deviation for normal distributions. The standard deviation can be defined from the inflection points of a normal distribution, which are a standard deviation away from the mean of the distribution. Using the inflection points at the left and right boundaries extends the notion of standard deviation for non-Gaussian distributions such as $p(x_{\text{meas}})$. The estimation procedure is illustrated with $p(x_{\text{meas}})$ in Fig. B.5a, where the inflection points used as estimates for the squeezing and antisqueezing levels are indicated with blue dashed lines. The squeezing (antisqueezing) level estimates are found by identifying the location of left-most maximum (right-most minimum) in the derivative of $p(x_{\text{meas}})$ in Fig. B.5b.

Bias of estimators

Let $\hat{x}^-$ and $\hat{x}^+$ represent the estimators of the squeezing (x^-) and antisqueezing (x^+) levels, where $\hat{x}^\pm$ correspond to the inflection points of $p(x_{\text{meas}})$. For finite σ, the Gaussian blurring shifts the inflection points from x^- and x^+ by an amount that scales with σ. The biases of the estimators are $E(\hat{x}^\pm) - x^\pm = \pm c^\pm \sigma$, where c^- and c^+ are constants. For distributions that are Gaussian convolutions, $c^\pm$ are typically less than one, depending on the behavior of distribution near the inflection points [20]. In Fig. B.6a, the analytical squeezing and antisqueezing levels for squeezed states (purple) are compared with the estimates obtained from the inflection points of the logarithmic squeezed quadrature variance PDFs convolved with a Gaussian distribution with $\sigma = 0.62$ dB (blue). The bias of the estimates are less than σ. In Fig. B.6b, the bias, or the percent difference of the (anti)squeezing estimates from the analytical (anti)squeezing levels, are plotted as a function of squeezing parameter for various efficiencies. The dashed lines correspond to $\pm\sigma$ from the analytical values. For high squeezing parameters, the biases approach a constant, approximately $\pm\sigma/2$. For squeezing parameters and efficiencies corresponding to squeezing and antisqueezing levels on the order of σ, the biases reach minima of approximately $\pm\sigma/3$. For low squeezing parameters, the biases approach $\pm\sigma$. This behavior is physically meaningful as the width of $g(x_{\text{noise}})$ represents a statistical noise floor. In the large sample size limit with $\sigma \to 0$, the biases approach zero and the inflection points coincide with the true squeezing and antisqueezing levels

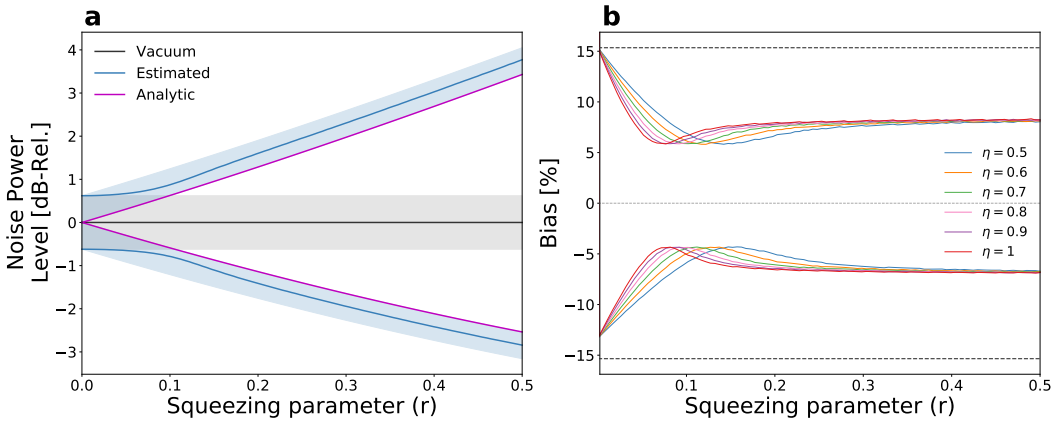

Figure B.6: Simulation of squeezing estimator bias. a) Noise power levels normalized to the mean shot noise level (black) as a function of squeezing parameter. The uncertainty in the shot noise level is depicted by the gray shaded region corresponding to $\pm\sigma$, where $\sigma = 0.62$ dB is the standard deviation of the shot noise power distribution. The squeezing (x^-) and antisqueezing (x^+) levels of a squeezed vacuum state are plotted in purple for unit measurement efficiency. The blue curves are the squeezing and antisqueezing level estimates for the observed squeezed vacuum state obtained from the inflection points of measured power distribution. The squeezing and antisqueezing estimates are within $+\sigma$ of the antisqueezing level and $-\sigma$ of the squeezing level, depicted by the blue shaded regions. b) The percent bias of the squeezing ($\hat{x}^-$) and antisqueezing ($\hat{x}^+$) estimates as a function of squeezing parameter, calculated as $100 \times (E(\hat{x}^\pm) - x^\pm)/x^\pm$.

as $p(x_{\text{meas}}) \to h(x_{\text{meas}})$.

Experimental results

The estimation procedure is applied to the experimental data from Fig. B.3b-e in Fig. B.7. The data are plotted again for reference in the first row. The histograms for the squeezed states (light blue) and vacuum states (orange) are shown in the second row. The kernal density estimates (KDEs) for the PDFs of the squeezed and vacuum states are plotted as the blue and black solid lines, respectively. The theoretical models for the squeezed state PDFs assuming a uniform phase distribution are plotted in purple. The theoretical models are calculated from Eq. B.11, where the integration is performed numerically.

To find the estimates for the squeezing and antisqueezing levels, the derivatives of the KDEs are calculated numerically. The derivatives of the KDEs of the squeezed

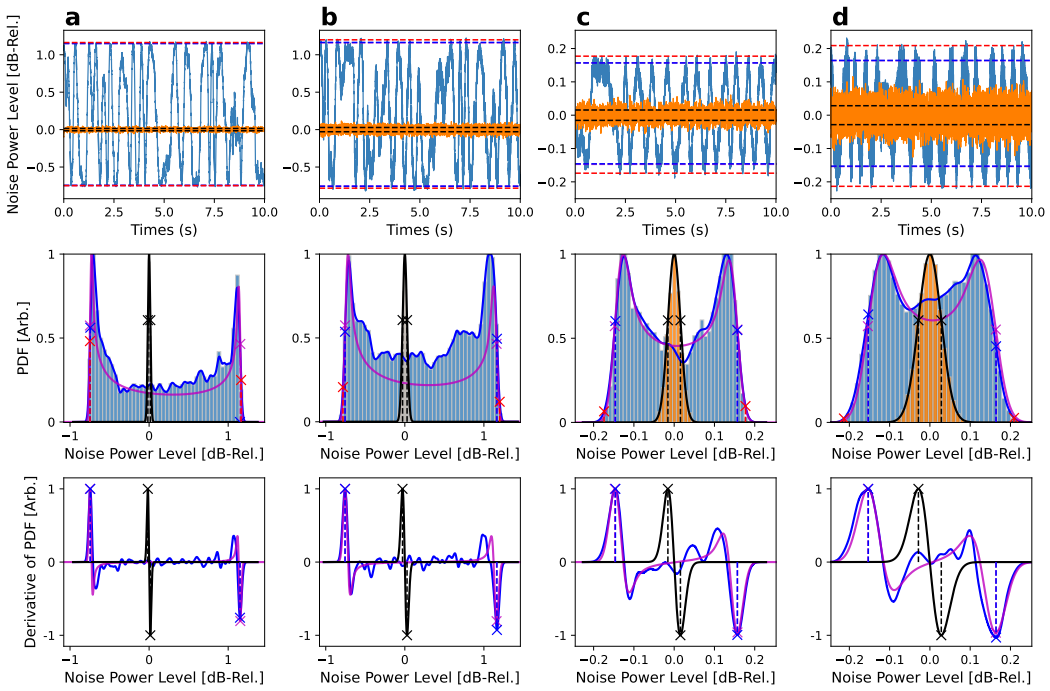

Figure B.7: Squeezing estimation with the frequency-domain measurements of squeezed light from Fig. B.3 for a) $r = 0.35$, VBW = 30 Hz, b) $r = 0.35$, VBW = 100 Hz, c) $r = 0.06$, VBW = 30 Hz, and d) $r = 0.06$, VBW = 100 Hz. First row: Noise power level traces of squeezed vacuum (light blue) and vacuum (orange) states relative to the mean shot noise level. The red dashed lines correspond to estimates of squeezing and antisqueezing levels from peak searching. The dark blue dashed lines correspond to the estimates of squeezing and antisqueezing levels from the inflection points of the noise power PDF of the squeezed vacuum data. The black dashed lines correspond to the inflection points of the shot noise power distribution. Second row: Histograms of the squeezed vacuum noise powers (light blue) and shot noise powers (orange). The Gaussian kernal density estimates (KDE) for PDFs of the squeezed vacuum and vacuum noise powers are shown in dark blue and black, respectively. The theoretical model for the squeezed vacuum PDF with the experimental squeezing parameter and system efficiency for a uniform phased distribution is shown in red. The inflection points of the squeezed vacuum KDE, vacuum KDE, and model are indicated with dark blue, black, and purple crosses, respectively. The squeezing and antisqueezing estimates from peak searching are indicated with red crosses. The histograms, KDEs, and model are rescaled to the maximum of the squeezed vacuum KDE. Third row: Derivatives of the squeezed vacuum KDE (blue), vacuum KDE (black), and theoretical model (purple), rescaled to the maximum of the vacuum KDE derivative, with the inflection points indicated with crosses.

states (blue) and vacuum states (black) are shown in the third row. The theoretical models for the squeezed state PDFs with uniform phase distribution are shown in purple. The theoretical models are calculated using the differentiation of convolution property,

$$\frac{dp(x_{\text{meas}})}{dx_{\text{meas}}} = \int_{-\infty}^{\infty} \frac{x - x_{\text{meas}}}{\sigma^2} h(x) g(x_{\text{meas}} - x) dx, \tag{B.12}$$

where the integration is performed numerically. For the squeezed state, the squeezing (antisqueezing) level is estimated as the noise power of the left-most maximum (right-most minimum). The same procedure is applied to the vacuum state KDE in order to obtain the noise floor. The procedure is also applied to the theoretical model to obtain the estimates for a uniform phase distribution.

In the first and second row, I compare the results of this procedure with those of the peak search algorithm from Fig. B.3. The squeezing and antisqueezing level estimates from the procedure and the peak search method are indicated with blue and red dashed lines, respectively. The shot noise floors are indicated with black dashed lines. The improvement over the peak search method is apparent for the low squeezing parameters, when the shot noise floor becomes significant. The peak search clearly overestimates the squeezing and antisqueezing levels, with estimates corresponding to the extrema of the noise powers as seen in the second row. Moreover, for the same squeezing parameter and effective efficiency, the peak search estimates change with the VBW setting, i.e. the standard deviation of the vacuum PDF, whereas the estimates from the procedure remain the same. This is because the peak search method relies on the tails of the PDF, and is therefore strongly influenced by the shape of the distribution. To demonstrate the robustness of this approach to experimental noise, I compare the estimates of this method to those of the theoretical model, indicated with purple dashed lines in the second row. Despite the non-uniformities in the KDEs, the estimates match closely with the theoretical model.

B.5 Discussion

I have demonstrated a method for estimating the squeezing and antisqueezing levels from the probability distribution of squeezed quadrature sample variances. The left and rightmost inflection points of the distribution are used as estimators of squeezing and antisqueezing. The squeezing parameter and system efficiency can estimated from the squeezing and antisqueezing levels from Eq. B.7. This method enables the estimation of squeezing in the the presence of high degrees of sampling

and phase noise and for low efficiencies, where the performance of characterization methods such as peak searching and optical homodyne tomography suffer. These estimators provide a well-defined measure for the left and right edges of the squeezed quadrature distribution in the presence of experimental noise sources such as phase and sampling noise, which blur the edges of the distribution. The bias of the estimators is typically within a standard deviation of the shot noise distribution and approaches zero for small shot noise distributions, in this case in the large sample size limit. This method is supported by theoretical modeling and experimental results.

References

[1] Alexander I Lvovsky. "Squeezed light." In: Photonics: Scientific Foundations, Technology and Applications 1 (2015), pp. 121–163.

[2] DT Smithey, M Beck, Michael G Raymer, and A Faridani. "Measurement of the Wigner distribution and the density matrix of a light mode using optical homodyne tomography: Application to squeezed states and the vacuum." In: Physical Review Letters 70.9 (1993), p. 1244.

[3] Alexander I Lvovsky and Michael G Raymer. "Continuous-variable optical quantum-state tomography." In: Reviews of Modern Physics 81.1 (2009), p. 299.

[4] Gerd Breitenbach, S Schiller, and J Mlynek. "Measurement of the quantum states of squeezed light." In: Nature 387.6632 (1997), pp. 471–475.

[5] Joel F. Tasker, Jonathan Frazer, Giacomo Ferranti, Euan J. Allen, Léandre F. Brunel, Sébastien Tanzilli, Virginia D'Auria, and Jonathan C. F. Matthews. "Silicon photonics interfaced with integrated electronics for 9 GHz measurement of squeezed light." In: Nature Photonics 15.1 (Jan. 2021), pp. 11–15.

[6] Alexander I Lvovsky. "Iterative maximum-likelihood reconstruction in quantum homodyne tomography." In: Journal of Optics B: Quantum and Semiclassical Optics 6.6 (2004), S556.

[7] Hauke Hansen, T Aichele, C Hettich, P Lodahl, AI Lvovsky, J Mlynek, and S Schiller. "Ultrasensitive pulsed, balanced homodyne detector: application to time-domain quantum measurements." In: Optics Letters 26.21 (2001), pp. 1714–1716.

[8] Hans-A. Bachor and Timothy C. Ralph. A guide to experiments in quantum optics. John Wiley & Sons, 2019.

[9] E Oelker, G Mansell, M Tse, J Miller, F Matichard, L Barsotti, P Fritschel, DE McClelland, M Evans, and N Mavalvala. "Ultra-low phase noise squeezed vacuum source for gravitational wave detectors." In: Optica 3.7 (2016), pp. 682–685.

[10] Florian Kaiser, Bruno Fedrici, Alessandro Zavatta, Virginia d'Auria, and Sébastien Tanzilli. "A fully guided-wave squeezing experiment for fiber quantum networks." In: Optica 3.4 (2016), pp. 362–365.

[11] Glen Cowan, Kyle Cranmer, Eilam Gross, and Ofer Vitells. “Asymptotic formulae for likelihood-based tests of new physics.” In: The European Physical Journal C 71 (2011), pp. 1–19.

[12] Louis Lyons. Statistics for nuclear and particle physicists. cambridge university press, 1989.

[13] Leonard Mandel and Emil Wolf. Optical coherence and quantum optics. Cambridge university press, 1995.

[14] Christian Weedbrook, Stefano Pirandola, Raúl García-Patrón, Nicolas J Cerf, Timothy C Ralph, Jeffrey H Shapiro, and Seth Lloyd. “Gaussian quantum information.” In: Reviews of Modern Physics 84.2 (2012), pp. 621–669.

[15] Jürgen Appel, Dallas Hoffman, Eden Figueroa, and A. I. Lvovsky. “Electronic noise in optical homodyne tomography.” In: Physical Review A 75.3 (2007), p. 035802.

[16] Rajveer Nehra, Ryoto Sekine, Luis Ledezma, Qiushi Guo, Robert M Gray, Arkadev Roy, and Alireza Marandi. “Few-cycle vacuum squeezing in nanophotonics.” In: Science 377.6612 (2022), pp. 1333–1337.

[17] Agilent Technologies. Spectrum Analysis Basics. 7th ed. Application Note 150. Originally published as Hewlett-Packard Application Note 150. Agilent Technologies. Santa Clara, CA, 2006. URL: https://www.keysight.com/zz-en/assets/7018-03115/application-notes/5965-7009.pdf.

[18] William G Cochran. “The distribution of quadratic forms in a normal system, with applications to the analysis of covariance.” In: Mathematical Proceedings of the Cambridge Philosophical Society. Vol. 30. 2. Cambridge University Press. 1934, pp. 178–191.

[19] Maurice S Bartlett and DG Kendall. “The statistical analysis of variance-heterogeneity and the logarithmic transformation.” In: Supplement to the Journal of the Royal Statistical Society 8.1 (1946), pp. 128–138.

[20] Steven M Kay. Fundamentals of statistical signal processing: estimation theory. Prentice-Hall, Inc., 1993.